THE JOURNAL OF PHYSICAL CHEMISTRY A
A JOURNAL OF THE AMERICAN CHEMICAL SOCIETY

pubs.acs.org/JPCA Article

Prediction of Phase State of Secondary Organic Aerosol Internally Mixed with Aqueous Inorganic Salts

Zechen Yu, Myoseon Jang,* and Azad Madhu

Cite This: J. Phys. Chem. A 2021, 125, 10198−10206 Read Online

ACCESS | Metrics & More | Article Recommendations | Supporting Information

ABSTRACT: In the presence of inorganic salts, secondary organic aerosol (SOA) undergoes liquid−liquid phase separation (LLPS), liquid−solid phase separation, or a homogeneous phase in ambient air. In this study, a regression model was derived to predict aerosol phase separation relative humidity (SRH) for various organic and inorganic mixes. The model implemented organic physicochemical parameters (i.e., oxygen to carbon ratio, molecular weight, and hydrogen-bonding ability) and the parameters related to inorganic compositions (i.e., ammonium, sulfate, nitrate, and water). The aerosol phase data were observed using an optical microscope and also collected from the literature. The crystallization of aerosols at the effloresce RH (ERH) was semiempirically predicted with a neural network model. Overall, the greater SRH appeared for the organic compounds with the lower oxygen to carbon ratios or the greater molecular weight and the higher aerosol acidity or the larger fraction of inorganic nitrate led to the lower SRH. The resulting model has been demonstrated for three different chamber-generated SOA (originated from β-pinene, toluene, and 1,3,5-trimethylbenzene), which were internally mixed with the inorganic aqueous system of ammonium−sulfate−water. For all three SOA systems, both observations and model predictions showed LLPS at RH <80%. In the urban atmosphere, LLPS is likely a frequent occurrence for the typical anthropogenic SOA, which originates from aromatic and alkane hydrocarbon.

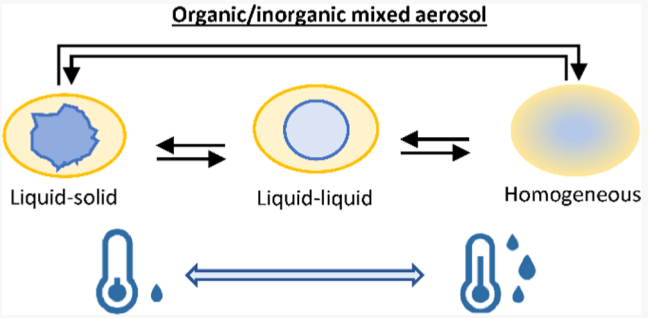

1. INTRODUCTION

Particulate matter (PM) is one of the major criteria pollutants that has a significant impact on human health[1,2] and climate forcing.[3,4] PM are often mixtures of water, inorganics, and organics, which are sourced from both primary emissions and secondary products formed through the atmospheric reaction of precursors.[4] Complex sets of inorganic and organic mixtures frequently show a dynamic phase transition such as liquid−liquid phase separation (LLPS), homogeneous aerosol phase (HAP), and liquid−solid separation under relevant environmental conditions. The aerosols scatter and absorb solar radiation, which may be changed during the phase transition. A recent study by Fard et al.[5] showed that aerosol optical properties can be modified due to the changing of aerosol phase state and consequently alter the aerosol radiation forcing. The changing of aerosol phase state also modifies their ability to act as nuclei for cloud droplets[6] and the atmospheric chemistry.[7]

As relative humidity (RH) cycles in the ambient atmosphere, the mixtures of organic and inorganic salts may experience phase transition.[8−14] Several technologies have been developed to study the aerosol phase state via direct or indirect observations. For example, Parsons et al.[15] developed an electrodynamic balance to study the crystallization of single droplets. Ciobanu et al.[16] used a Raman microscope coupled with a heating/cooling cell for the measurement of aerosol phase state. The optical reflectance microscope mounted with a temperature and RH controlled flow cell was also adapted to study the aerosol phase state of particles with diameter ranges from 10 to 300 μm.[10,14,17,18] A more precise technique using optical tweezers was recently developed by Rafferty et al.[19] to study the aerosol phase state of single particles with nanometer size. The recent study by Ohno et al.[20] used a fluorescence aerosol flow tube spectroscopy to characterize the phase state of inorganic and organic mixed submicron particles (100−200 nm) containing poly(ethylene glycol), ammonium sulfate, and sodium chloride.

The aerosol phase state and the aerosol phase separation relative humidity (SRH) of various organic−inorganic mixtures were predicted previously using a semiempirical equation in terms of the oxygen to carbon (O/C) ratio of organic.[10,14,17,18] The resulting model is a rough approximation of the aerosol phase state and is robust for the predicting of aerosols with extremely low O/C ratio (<0.3) or extremely high O/C ratios

Received: July 30, 2021
Revised: November 8, 2021
Published: November 19, 2021

https://doi.org/10.1021/acs.jpca.1c06773
J. Phys. Chem. A 2021, 125, 10198−10206

(>0.8). For typical ambient aerosols, which O/C ratio often ranges from 0.3 to 0.8,[21] the predicted aerosol phase state remains a large uncertain. In addition, aerosol acidity can also impact the phase transition of inorganic/organic mixed aerosols.[12] Therefore, a more elaborate prediction model with the consideration of various physicochemical parameters of organic and inorganic compounds is needed.

Machine learning (ML) can provide a useful tool for the semiempirical prediction of aerosol properties. Deep learning neural network, a typical machine learning method, has been increasingly applied in the prediction of air qualities and emissions.[22−27] Deep learning can have customized structures for different goals, such as classification, regression, and prediction. On the other hand, ML model could be overfitted with a small database and has generally more complex model parameters compared to traditional regression models.

In this study, SRH of various organics that were internally mixed with different inorganic compositions was observed using the optical microscope, which was mounted with a temperature and humidity-controlled flow cell. The newly added data in this study and the reported literature values[8,10,12,17,28] were used to derive a multilinear regression model to predict SRH as a function of various physicochemical parameters (i.e., salt compositions, inorganic to organic ratios, O/C ratios of the organics, and molecular weight). In addition, the prediction of effloresce RH (ERH) of the inorganic species, which was semiempirically estimated using a deep neural network as a function of inorganic compositions, was applied to determine whether SRH is higher than ERH. The model was also demonstrated by measuring SRH for three-chamber-generated secondary organic aerosol (SOA) (toluene, 1,3,5-trimethylbenzene, and β-pinene) mixed with inorganic salts (i.e., ammonium hydrogen sulfate). Toluene and 1,3,5-trimethylbenzene are abundant in the urban environment,[29] while β-pinene is one of the important biogenic SOA precursors in rural areas.

2. MATERIALS AND METHODS

2.1. Measurement of Aerosol Phase State. Table 1 lists model organic compounds used for the measurement of aerosol phase state in the presence of various inorganic compositions. Four carboxylic acids and one alcohol were investigated for the study of the aerosol phase state. All of the organic chemicals used for the experiments were purchased from Sigma-Aldrich: mesaconic acid (99%), azelaic acid (98%), suberic acid (98%), 1,4-butanediol (99%), and adipic acid (99%). The O/C ratio for the selected organic species ranges from 0.44 to 0.8. A detailed experimental condition for the observations of SRH used in this study is listed in Table S1 (Supporting Information).

Figure S1 illustrates the experimental setup for the measurement of aerosol phase state using the microscope (B120, Amscope Inc.) mounted with a specifically fabricated flow cell. The organic species were mixed with different inorganic salts in 3 mL of water/methanol (1:1 in volume). The aerosols were generated by passing clean air through a nebulizer (Pari LC star, Starnberg, Germany) and impacting on a 13 mm diameter transparent Teflon film. Methanol was quickly evaporated during the nebulization. The Teflon film was immediately put into the flow cell for the observation of the aerosol phase state. An inline water vapor analyzer (RH-300, Sable Systems International Inc.) was used to monitor RH inside the flow cell. The inline RH sensor was calibrated using

Table 1. Experimental Conditions for the Measurement of Phase Separation Relative Humidity (SRH) of Model Organic Compounds

exp no.	compounds	O/C	f_{anion}[a]	IOR[b]	average SRH (%)[c]
1	mesaconic acid	0.80	0.50	2.07	53.0 ± 3.5
2	mesaconic acid	0.80	0.59	1.92	0
3	mesaconic acid	0.80	0.67	0.97	0
4	azelaic acid	0.44	0.50	1.92	>95.0
5	azelaic acid	0.44	0.67	0.56	91.7 ± 2.1
6	azelaic acid	0.44	0.86	1.95	88.0 ± 2.7
7	suberic acid	0.50	0.50	2.02	>95.0
8	suberic acid	0.50	0.67	2.11	78.3 ± 3.8
9	suberic acid	0.50	0.80	1.97	76.7 ± 5.1
10	suberic acid	0.50	1.00	0.50	75.3 ± 4.5
11	1,4-butanediol	0.50	1.00	0.94	0
12	1,4-butanediol	0.50	0.50	1.90	62.3 ± 2.5
14	adipic acid	0.67	0.50	1.92	90.0 ± 2.0
15	adipic acid	0.67	1.00	1.96	51.3 ± 3.5
16	adipic acid	0.67	0.71	1.98	69.2 ± 2.6
17	adipic acid	0.67	1.00	2.08	54.0 ± 4.7
18	adipic acid	0.67	0.84	1.98	57.7 ± 3.6
19	adipic acid	0.67	0.91	1.94	57.4 ± 4.1
20	adipic acid	0.67	0.55	2.00	79.5 ± 2.6
21	adipic acid	0.67	0.63	2.00	72.0 ± 3.0

[a]f_{anion} is the fraction of anion valence charges to total ions valence charges. [b]IOR is the mass ratio of dry inorganic products to organic products. [c]The averaged SRH and the associated errors were calculated by three replicates. SRH equal to 0 when LLPS was not observed for RH greater than ERH of the inorganic species.

dry nitrogen gas (RH = 0%) and a bubbler flask, which was saturated with water vapor at a temperature lower than the temperature of the inline RH sensor (RH = 100%). RH was controlled by manipulating the airflow (~1 L min^{-1}) by passing clean and dry air through a water bubbler. The initial RH in the flow cell was set to ~95% after inserting the particle impacted Teflon film and allow to equilibrate for 10 min. Then, RH decreased at a rate of 0.8−1% per minute. The temperature of the flow cell was ~298 K during all of the experiments. The sizes of the observed particles are ranged from 20 to 30 μm before adjusting RH. The video of the aerosols was recorded at 5 frames per second until RH reached 5% or ERH. The measurements were repeated three times for each combination of the organic compound and inorganic compositions. The measurement method and the aerosol equilibrium time were examined by measuring the ERH of pure ammonium sulfate inorganic particles. The estimated ERH of ammonium sulfate particle is 45.5 ± 3.0%, which is similar to the reported value, ~45% for 20 μm of particles.[30−33] An example of the optical image for the aerosol phase transition is shown in Figure S2.

2.2. SOA Generated Using an Outdoor Photochemical Reactor. SOA was produced from the photooxidation of three different hydrocarbons: β-pinene, toluene, and 1,3,5-trimethylbenzene using the Atmospheric PHotochemical Outdoor Reactor (UF-APHOR) dual chamber (52 m^3 each) located at the University of Florida in the presence of NO_x. The detailed information for the operation of the outdoor photochemical reactor has been described in the previous studies.[34−38] Briefly, the hydrocarbons were evaporated into the outdoor chamber with heating. Four hundred parts per billion of nonreactive CCl_4 (Sigma-Aldrich; ≥99.5%)

https://doi.org/10.1021/acs.jpca.1c06773
J. Phys. Chem. A 2021, 125, 10198−10206

Table 2. Chamber Experimental Conditions for SOA Samples to Measure SRH

precursors	date[a]	experimental conditions				SOA yield[b] (%)
		consumed hydrocarbon (ppb)	HC/NO_x (ppbC/ppb)	temp. (K)	RH (%)	
β-pinene	03/04/2021-E	311	23.1	280−308	29−90	5.9
toluene	03/14/2021-E	792	22.1	286−315	21−89	10.9
1,3,5-trimethyl-benzene	03/14/2021-W	684	21.8	287−315	27−94	4.45

[a]"E" and "W" denote the east side and west side of the UF-APHOR outdoor photochemical dual reactor, respectively. [b]SOA yield is estimated using the concentration of total organic matter normalized by the consumption of hydrocarbons. The total organic matter concentration was corrected by the particle loss to the chamber wall. The SOA yields were estimated at the end of each experiment.

was used as the indicator for chamber dilution. Hydrocarbons and NO (2% in N_2, Airgas Inc.) were introduced into the smog chamber before sunrise. The concentration of gas-phase HCs was monitored by a gas chromatography flame ionization detector (GC-FID) (7820A, Agilent Technologies, Inc.). The concentrations of ozone and NO_x were continuously monitored by a photometric ozone analyzer (400E, Teledyne Technologies, Inc.) and a chemiluminescence NO/NO_x analyzer (T201, Teledyne Technologies, Inc.), respectively.

The particle size distribution was monitored using a scanning mobility particle sizer (SMPS 3080, TSI Inc.). The meteorological factors, such as temperature, relative humidity (RH), and sunlight intensity, were monitored both inside and outside of the smog chamber using a hygrometer (CR1000 measurement and control system, Campbell Scientific Inc.) and an ultraviolet radiometer (TUVR, Eppley Laboratory Inc.), respectively. The concentration of organic carbon in aerosol was monitored using an organic carbon/elemental carbon aerosol analyzer (OC/EC model 4, Sunset Laboratory Inc.) for every 50 min. The aerosols were also monitored by an aerosol chemical speciation monitor (ACSM, Aerodyne Research Inc.). The concentration of OM produced in the chamber was corrected for both chamber dilution using the dilution factor and the particle loss to the chamber wall using a particle loss factor. The resulting ACSM compositions were used to estimate the organic nitrate formation. SOA yields (Y) were then calculated as the maximum concentration of OM divided by the consumption of HC precursors. The detailed experimental conditions of outdoor chamber experiments are summarized in Table 2.

SOA was collected by sampling onto a 13 mm Teflon-coated glass fiber filter (Emfab TX40 HI20 WW; Pallflex Corp., Putnam). The filters were weighted using an analytical balance (MX5; Mettler-Toledo Ltd., England) before and after the sampling. After the collection of samples, the filters were immediately extracted by 3 mL of water/methanol mixture (1:1 in volume) and then internally mixed with inorganic aqueous salts. The extraction efficiency was calculated by the weighted dry filter mass before and after the extraction. The estimated extraction efficiency of filter samples was nearly 100%. The inorganic/organic mixture was used for the measurement of SRH. The O/C ratio of the chamber-generated SOA was calculated using the filter mass, the organic carbon concentration by OC/EC, the reference value of H/C ratio (1.1−1.6),[39,40] and the fraction of organic nitrate measured by ACSM (5−10%). The detailed calculation method is described in Section S3 in the Supporting Information.

3. RESULTS AND DISCUSSION

3.1. Efflorescence Relative Humidity Prediction Using a Deep Neural Network. The phase state data collected in this study contained both LLPS particles, homogenous liquid phase particles, and solid-core liquid-shell particles. In particular, the SRH of the solid-core liquid-shell particle was lower than the ERH and recorded as 0%. Thus, the solid-core liquid-shell particle cannot be directly applied to the prediction of aerosol phase state and was excluded from phase state data. In this study, the ERH of the salted aqueous solution was semiempirically predicted for inorganic salts frequently found in ambient air (i.e., ammonium, sulfate, and nitrate ions). In general, the prediction of ERH for a multicomponent aerosol is much more complicated than that of pure inorganic salt. The crystallization of a multicomponent salt may involve both heterogeneous nucleations of salts and homogenous nucleation depending on the interaction between ions.[41,42] Owing to its nonlinearity, a machine learning model by a deep neural network approach was employed to predict ERH of atmospherically abundant inorganic salts, which comprise ammonium, sulfate, and nitrate ions. Two inputs were used: the molar fraction of nitrate to total anions (f_{nitrate}) and the fraction of anion charges to total ions charges except proton (i.e., f_{anion} = 0.5 for ammonium sulfate and f_{anion} = 1 for sulfuric acid)

$$f_{\text{anion}} = \frac{n(NO_3^-) + 2 \times n(SO_4^{2-})}{n(NO_3^-) + 2 \times n(SO_4^{2-}) + n(NH_4^+)} \quad (1)$$

For the derivation of the model, the literature data were used (Table S3).[30,32,33] Data augmentation was also applied by introducing random noise (<5%) within the uncertainties of input variables. After then, the database was randomly divided into a training set (120 cases) for fitting of model parameters and a validation set (30 cases) for the evaluation of model performance.

The architecture of the neural network used in this study is shown in Figure S4 in the Supporting Information. Two hidden layers were included with five neurons in total. The detailed information of the neural network used in this study is explained in Section S2. The number of neurons was optimized by minimizing the neurons without decreasing the prediction accuracy. The neural network was trained based on the Keras model using TensorFlow 2 as the backend (https://keras.io). The mean squares errors (MSE) between observations and predictions were used as the loss function for the evaluation of training performance. The training and validation were performed on an NVIDIA Tesla K80 GPU cloud machine provided by the Microsoft Azure machine learning studio. The model was trained for 1000 epochs or until the validation loss reached the minimum. Figure S5 shows the model performance on the training set and the validation set. As shown in Figure S5a, the MSE between the training set and the validation set has no significant difference indicates that the model is robust. Figure S5b shows the predicted ERH of

https://doi.org/10.1021/acs.jpca.1c06773
J. Phys. Chem. A 2021, 125, 10198−10206

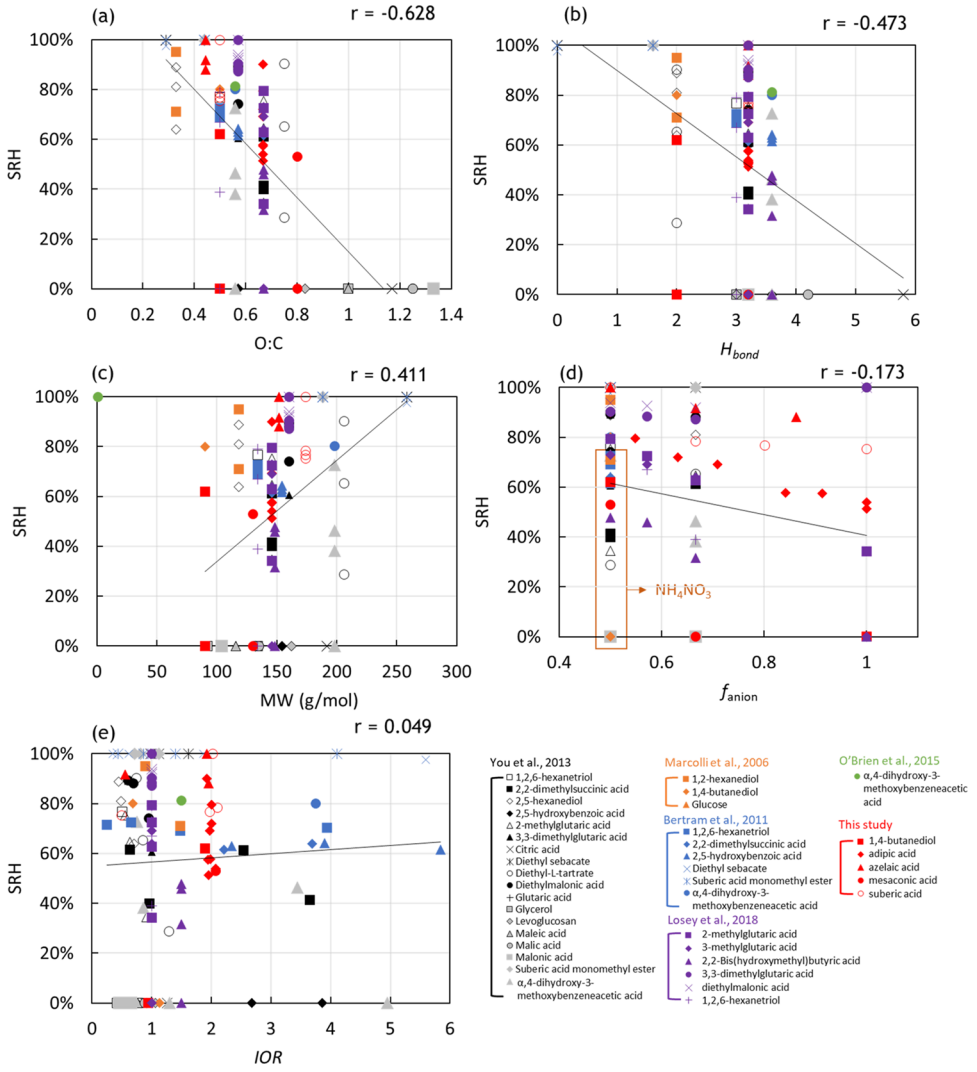

Figure 1. Observations of phase SRH vs (a) O/C ratios, (b) hydrogen bond parameter (H_{bond}), (c) molecular weight (g mol^{-1}), (d) anion compositions (f_{anion} in eq 1), and (e) inorganic to organic dry mass ratio (IOR). r is the calculated correlation coefficient. Observed data were obtained from an optical microscope data of this study and the literature data (Table S1).

validation data vs the observations. Overall, the ERH of the inorganic salts in the database is well predicted by the generated model (R^2 = 0.913).

3.2. Correlation between Observed SRH and Physicochemical Parameters. For the inorganic/organic mixed aerosol, LLPS occurs when the organic concentration exceeds its maximum solubility at a given inorganic aqueous solution. The maximum solubility of an organic component in the inorganic and organic mix is closely related to their interaction energy as well as mixing entropy. The interaction energy can be influenced by organic physicochemical parameters (i.e., polarity) and inorganic compositions that are modulated by the type of ions and humidity (i.e., aerosol water content). The O/C ratio is commonly used as a simple proxy for the polarity of organic species. Additionally, the hydrogen bond parameter (H_{bond}) significantly impacts the solubility of organic species in the salted aqueous phase, which is closely related to maximum solubility. The H_{bond} value is estimated mainly for a hydroxyl group (number of OH) and a carboxylic acid group (1.6 × number of COOH).[34,38] Molecular weight (MW, g mol^{-1}) negatively influences organic solubility because the larger molecule needs a greater mixing entropy to mix with water molecules.[43,44] For inorganic compositions, in a similar manner to the prediction of ERH (Section 3.1), f_{anion} and $f_{nitrate}$ were employed in the predictive model.

To investigate the influence of aerosol's physicochemical parameters on phase state, the SRH data were plotted to O/C ratios (Figure 1a), MW (Figure 1b), H_{bond} (Figure 1c), f_{anion} (Figure 1d), and inorganic to organic dry mass ratio (IOR) (Figure 1e) for various organic and inorganic mixtures. SRH data were selected for those when SRH was higher than the ERH of inorganic salts. The ERH of inorganic salts was predicted by the model derived in Section 3.1. Among total 136 data (Table S1), including literature values[8,10,12,17,28] and the measurements of this study, 117 data were feasible when SRH was higher than the predicted ERH of the inorganic salts. Within the feasible data, 89 mixtures undergo LLPS over the experimental RH ranges and the others remain in a homogeneous phase.

As seen in Figure 1, the O/C ratios of organic compounds exhibit the strongest correlation with the observed SRH (correlation coefficient: r = −0.628). For the O/C ratio greater than 0.8, aerosol is homogeneous in most cases. Similar to the results reported by previous studies,[10,11,17,45] when the O/C

https://doi.org/10.1021/acs.jpca.1c06773
J. Phys. Chem. A 2021, 125, 10198−10206

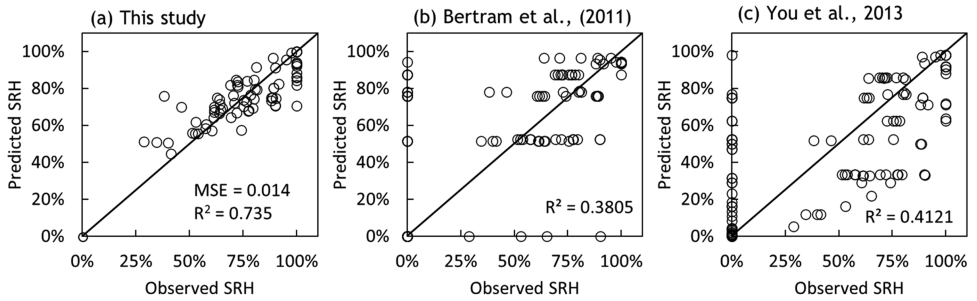

Figure 2. Observed SRH vs the predicted SRH using the derived equation from (a) this study, (b) the study by Bertram et al.,[17] and (c) the study by You et al.[10] The observed data were obtained from an optical microscope data of this study and the literature (Table S1).

ratio ranges between 0.4 and 0.8, the role of O/C ratios on SRH is somewhat uncertain, indicating that SRH is also impacted by other physicochemical parameters. In general, the higher SRH appears with the lower O/C ratio, which accords with the previous laboratory studies.[10,46] In a similar matter, the H_{bond} parameter is negatively correlated with the observed SRH (r = −0.473 in Figure 1b). MW, however, showed a weakly positive correlation with the observed SRH (r = 0.411 in Figure 1c) due to the poor solubility of the organic compound with a large MW.

Acidic aerosols appeared in ambient, but their SRH were not well studied. Thus, in this study, the SRH data for acidic aerosols (f_{anion} between 0.67 and 1 in Figure 1d) was newly added. LLPS was observed when aerosol pH is close to neutral, which homogeneous phase appeared at a lower pH. For example, the SRH dropped from 90 to 54% when f_{anion} mixed with adipic acid increased from 0.5 to 1 based on the experimental data of this study. The more acidic aerosol was more hygroscopic, lowering ionic strength. This tendency was also consistent with the previous observations by Losey, Ott, and Freedman.[12] However, the f_{anion} parameter was not enough to represent the impact of inorganic composition on SRH. In the f_{anion} scale, f_{anion} of ammonium nitrate is the same as that of ammonium sulfate. In general, ammonium nitrate is more hygroscopic than ammonium sulfate. The study by You, Renbaum-Wolff, and Bertram[10] reported the lower SRH of the ammonium nitrate/organic compound mix than that of the ammonium sulfate/organic compound mix. Therefore, $f_{nitrate}$ was introduced to the model. In addition, the IOR values of this study were mostly ranged between 0.5 and 2 and weakly correlated with SRH (r = 0.094, Figure 1e).

To investigate the correlation between SRH and model parameters in the absence of the influence by the inorganic composition, the data with ammonium sulfate (59 cases) were chosen, as seen in Figure S3. All correlation coefficients (r values) were enhanced compared to those in Figure 1. The correlation of the O/C ratio with SRH was slightly enhanced from −0.628 to −0.639 (Figure S3a). However, a significant improvement appeared in the correlation coefficients of SRH with other parameters such as H_{bond} (−0.473 to −0.633 in Figure S3b), MW (0.411−0.571 in Figure S3c), and IOR (0.049 to −0.244 in Figure S3d). The previous study by You and Bertram[47] showed that the SRH of inorganic−organic mixed aerosol does not have a strong dependence on organic MW. However, by choosing more diversified chemical species and various experimental conditions in this study, MW showed a moderate dependence on SRH. Overall, O/C ratios showed the strongest correlation to observed SRH data, followed by H_{bond} and MW. Inorganic-related parameters, f_{anion} and IOR ratios, are somewhat weak but still statistically significant.

3.3. Semiempirical Model to Predict SRH. A multilinear regression model was derived to predict the SRH of organic aerosol internally mixed inorganic salts using the physicochemical properties of organic species and inorganic compositional parameters. As discussed in Section 3.2, six model parameters, O/C, H_{bond}, MW, f_{anion}, $f_{nitrate}$, and IOR were included to fit a polynomial equation to the data demonstrated in Figure 1. The resulted regression model is described as

$$\begin{aligned} \mathrm{SRH} = {} & 1.3271 - 0.599 \times \mathrm{O/C} - 0.028 \times H_{bond} \\ & + 0.00044 \times \mathrm{MW} - 0.300 \times f_{anion} - 0.221 f_{nitrate} \\ & - 0.022 \times \mathrm{IOR} \end{aligned} \quad (2)$$

All organic and inorganic parameters except MW are negatively correlated with SRH. The higher organic solubility in the salted aqueous phase generally reduces SRH. Organic hydrophilicity increases with increasing O/C ratios and H_{bond}. Inorganic hygroscopicity increases with increasing f_{anion} and $f_{nitrate}$. The higher IOR increases an aerosol water content potential. However, the organic compound with a large MW increases the combinational mixing energy with water molecules and reduces its solubility in the salted aqueous phase.

The derived semiempirical model was applied to the prediction of SRH for all data listed in Table S1, which included any aerosol phase state: LLPS particle, homogeneous phase aerosol, and solid-core liquid-shell particle. The predicted SRH was plotted to the observed SRH in Figure 2a. To predict SRH, all parameters, O/C, f_{anion}, $f_{nitrate}$, H_{bond}, MW, and IOR, were statistically significant, showing that all p-values were less than 0.05. The predictability of the SRH ranging from 50 to 80% was relatively high. For the SRH larger than 80%, the model slightly underestimates SRH, while for the SRH less than 50%, the regression model tends to overestimate SRH. The SRH prediction using the derived equations from previous studies[10,17] are also plotted in Figure 2b,c. The predicted SRH from this study has much better accuracy with R^2 = 0.735 (MSE = 0.014) than the SRH predicted using previously derived equations ($R^2 \approx 0.4$), especially for the cases where SRH is lower than the ERH of the inorganic compounds.

3.4. Prediction of SRH for SOA Internally Mixed with Inorganic Salts. The SRH predictive model that was derived from model compounds was extended to the SOA internally mixed with inorganic salts. Unlike the model compounds (pure organic compounds), SOA comprises various organic products that differ in MW, O/C ratios, and H_{bond} parameter. In this

https://doi.org/10.1021/acs.jpca.1c06773
J. Phys. Chem. A 2021, 125, 10198−10206

study, the SRH values of the chamber-generated SOA (oxidized from β-pinene, toluene, and 1,3,5-trimethylbenzene), which were internally mixed with the ammonium sulfate system (f_{anion} = 0.5−0.8), were simulated against observations based on microscopic data. The SOA model parameters comprising MW, O/C ratios, and H_{bond} were estimated using the aerosol composition predicted using the UNIPAR SOA model.[34,38,48,49] The detailed description of organic parameters is shown in Section S3 and Table S4 in the Supporting Information. For all SOA data, LLPS was observed when RH was less than 90%. The predicted SRH of three aerosol mixtures range from 0.7 to 0.95 as seen in Figure 3. For β-pinene SOA and toluene SOA, the simulated SRH was underestimated compared to the observations. SOA products contain multifunctional complex structures and oligomeric products, as discussed in Section S3. The MW and H_{bond} parameters of some SOA products are beyond the data employed in the predictive SRH model (eq 2) and this may hinder the predictability of the SOA's phase state.

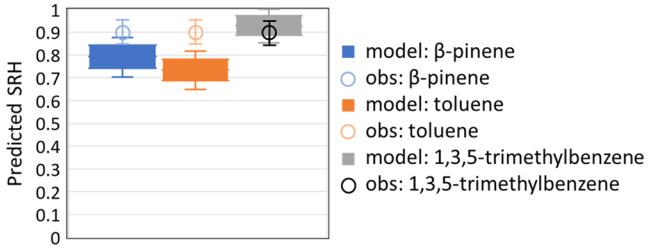

Figure 3. Modeled (model) and observed (obs) SRH for the three different chamber-generated SOA: β-pinene, toluene, and 1,3,5-trimethylbenzene with various IOR (0.2−0.8) and f_{anion} (0.5−0.8). The uncertainty of the predicted SRH using eq 2 was determined based on the uncertainties in physicochemical parameters (O/C ratio, MW, and H_{bond} in Table S3) of each SOA produced in the chamber. The SOA is internally mixed with inorganic salts during the SRH measurements.

4. MODEL SENSITIVITIES

The sensitivity of the predicted SRH to model parameters (i.e., MW, O/C, H_{bond} parameter, f_{anion}, $f_{nitrate}$, and IOR) was evaluated by changing of each model parameters while set other parameters to the reference value (Figure 4). The sensitivity of the predicted SRH is tested for O/C from 0 to 1, MW from 100 to 300 g mol^{-1}, H_{bond} from 0 to 5, f_{anion} from 0.5 to 1, $f_{nitrate}$ from 0 to 1, and IOR from 0 to 10. For the reference values to the model equation, MW was set to 200 g mol^{-1}, f_{anion} to 0.75 (slightly acidic), $f_{nitrate}$ to 0 (no nitrate), IOR to 1, and H_{bond} to 1 (averaged for the organic mixture). The phase state transition boundary in counter mappings was plotted when the predicted SRH was higher than the predicted ERH of the inorganic species. The noncolor region (white color) represents the case where the predicted SRH is less than the ERH of inorganic salts. When the O/C ratio is very high (>0.8), SRH is nearly 0 and the aerosol is homogeneous above ERH.

As discussed in Section 3.3, organic and inorganic parameters except MW are negatively correlated with SRH (eq 2). Therefore, the SRH decreases in the diagonal direction in the counter map between O/C ratios and all other parameters (Figure 4B−E) except the counter map between O/C ratios and MW (Figure 4A). The rectangular box in

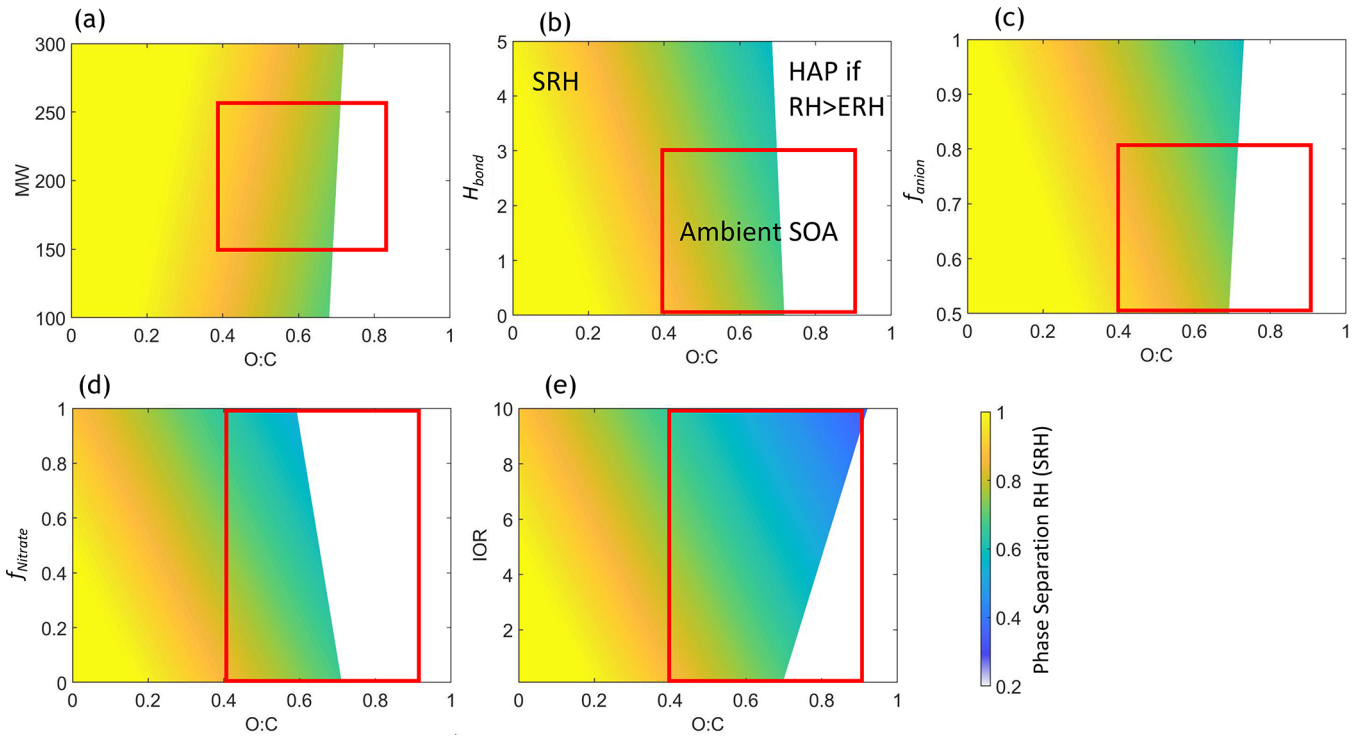

Figure 4. Counter mapping for the sensitivity of the predicted SRH to various model parameters: (a) O/C ratios vs MW (100−300, g mol^{-1}), (b) O/C ratios vs hydrogen-bonding (H_{bond}) parameter (0−5), (c) O/C ratios vs f_{anion} (0.5−1), (d) O/C ratios vs $f_{nitrate}$ (0−1), and (e) O/C ratios vs inorganic to organic dry mass ratio (IOR = 0.1−10). The rectangular box indicates the upper and lower boundary of the ambient SOA mixed with an aqueous salted solution. For the reference values, MW was set to 200 g mol^{-1}, f_{anion} to 0.75, $f_{nitrate}$ to 0, IOR to 1, and H_{bond} to 1.

https://doi.org/10.1021/acs.jpca.1c06773
J. Phys. Chem. A 2021, 125, 10198−10206

Figure 4 illustrates the predicted SRH within the upper and the lower boundaries of two model parameters relevant to the ambient aerosols containing SOA and aqueous inorganic salts. In the ambient SOA region, SRH is relatively high except for high O/C ratios and large $f_{nitrate}$. The high SRH suggests that the organic and inorganic mix prefers LLPS for the low to mid-RH conditions (<0.7) in ambient air. The variation of IOR is large in ambient aerosol ranging from 0.1 to 10[50−52] and its corresponding SRH change is also large ranging from 0.4 to 0.8. The predicted SRH decreases by 10% with decreasing IOR from 0.5 to 2. The predictions within this range are well in accord with the observations reported previously.[45]

5. ATMOSPHERIC IMPLICATIONS AND UNCERTAINTIES

The polynomial equation derived in this study using organic physicochemical parameters (i.e., O/C ratios, MW, and H_{bond}) and the parameters related to inorganic salt compositions (i.e., f_{anion}, $f_{nitrate}$, and IOR) was able to reasonably predict SRH of the organics internally mixed with aqueous inorganic salts (R^2 = 0.73, Figure 2). The resulting model was also suitable to predict the SRH of the three different SOA/inorganic salt mixes (i.e., SOA from β-pinene, toluene, and 1,3,5-trimethylbenzene in Figure 3). For the aerosol that undergoes the crystallization of salts (ammonium, nitrate, and sulfate), the ERH was predicted using a neural network model (Figure S5). The sensitivity test shows that the predicted SRH is strongly correlated with O/C ratio, MW, and H_{bond} parameters but relatively weakly correlated with f_{anion}, $f_{nitrate}$, and IOR (Figure 4).

The ambient aerosol consists of complex oxygenated organic products, which originate from the atmospheric oxidation of both biogenic and anthropogenic hydrocarbons. In general, isoprene SOA is very hydrophilic with a higher O/C ratio (0.75−0.9).[21] The predicted SRH using eq 2 suggested that the isoprene SOA internally mixed with inorganic salts will likely form a homogeneous aerosol phase. This simulation also accords with previously reported studies.[34,53−58] Both terpene SOA and aromatic SOA products, however, are less hydrophilic than isoprene SOA, leading LLPS in the presence of inorganic aqueous salts (Figure 3). On the other hand, the O/C ratio of SOA can be increased as it undergoes photochemical aging process.[21] Thus, the aerosol could also transformed from LLPS to be in a homogeneous phase under the relevant environmental conditions. For the urban environments, SOA is primarily produced from the oxidation of aromatic and alkane hydrocarbons, which originate from anthropogenic emissions. Thus, this SOA will likely form LLPS in the presence of an aqueous salted solution.

In addition to aerosol compositions, the phase state of an ambient aerosol can be significantly impacted by relative humidity. For instance, under dry regions (i.e., western USA), where RH is generally lower than ERH at daytime and it is also lower than deliquescence RH at nighttime, the aerosol mixture may undergo solid−liquid phase separation. For humid regions, such as the southeastern US in summer and coastal regions, inorganic salts are deliquesced and form the homogeneous phase at nighttime and LLPS at daytime.

The prediction of ERH can significantly improve the accuracy of the SOA model due to the pathway of SOA formation via the aqueous reactions of organic species. For example, chamber studies showed that SOA formation considerably decreases at ERH when RH decreases during daytime.[34,38,49] Owing to the mitigation of SO_2 emissions in recent years (reduced more than 74% from 2010 to 2020; https://www.epa.gov/air-emissions-inventories/air-pollutant-emissions-trends-data), sulfate in ambient aerosols has been gradually reduced. However, a high fraction of ammonium nitrate can appear in an ambient aerosol under the low sulfate.[59] The increased nitrate may lower the SRH owing to its large hygroscopicity when it is mixed with organics and increase the frequency of the homogeneous phase. Up to date, there is a lack of SRH data in nitrate blended with sulfate and need to be included in the future for better predicting SRH.

The uncertainties in the SRH prediction are associated with the experimental techniques, the database, and the goodness-of-fit of parameterizations. To observe aerosol phase transition, the microscope mounted with the flow cell has also been frequently used in previous studies due to its simplicity.[8−10,12,14] This microscopy observation of the aerosols is limited to a large particle diameter greater than 1 μm due to the limitation in the optical lens. However, an ambient aerosol is frequently found in submicron particles (<1 μm), which phase state can be different from that in large particles. For example, the previous study by Altaf et al.[60] suggested that small particles (<0.2 μm) cannot overcome the activation energy to form a new phase and thus tend to be homogeneous. A better observation technique is essential to provide the database relevant to ambient aerosol and improve the predictability of SRH. Hundreds of SRH data were included in the model derivation of this study, but the resulted model is still limited to predicting SRH within the ranges of the database. The ambient aerosol, however, can include the higher IOR or the higher H_{bond} regions than those in this study (Figure 1). Most SRH observations that are available from the literature are organic acid and ester, which may not represent the actually ambient organic aerosol. The derived prediction model from a limited database could be biased when applying it to the ambient aerosol. For the case where SRH is a nonlinear function of the physicochemical parameters (i.e., O/C ratio >0.8), the multiregression model may not be the best fitting model for the SRH. Therefore, the prediction model could be improved in the future by considering the nonlinearity correlation between SRH and other physicochemical parameters.

■ ASSOCIATED CONTENT

Supporting Information

The Supporting Information is available free of charge at https://pubs.acs.org/doi/10.1021/acs.jpca.1c06773.

Measurement of aerosol phase separation relative humidity (SRH); semiempirical model to predict efflorescence relative humidity of inorganic salts; and aerosol phase state and phase transition for the SOA internally mixed with the salted aqueous solution (PDF)

■ AUTHOR INFORMATION

Corresponding Author

Myoseon Jang − *Department of Environmental Engineering Sciences, University of Florida, Gainesville, Florida 32611, United States;* orcid.org/0000-0003-4211-7883; Email: mjang@ufl.edu

https://doi.org/10.1021/acs.jpca.1c06773
J. Phys. Chem. A 2021, 125, 10198−10206

Authors

Zechen Yu − *Department of Environmental Engineering Sciences, University of Florida, Gainesville, Florida 32611, United States;* orcid.org/0000-0002-6763-0520

Azad Madhu − *Department of Environmental Engineering Sciences, University of Florida, Gainesville, Florida 32611, United States*

Complete contact information is available at: https://pubs.acs.org/10.1021/acs.jpca.1c06773

Notes

The authors declare no competing financial interest.

■ ACKNOWLEDGMENTS

This research was supported by the National Science Foundation (AGS1923651), the FRIEND (Fine Particle Research Initiative in East Asia Considering National Differences) Project through the National Research Foundation of Korea (NRF), funded by the Ministry of Science and ICT (2020M3G1A1114562), the National Institute of Environmental Research (NIER2020-01-01-010), and the Microsoft AI for Earth (AI4E-1844-N6Q4-21010409).

■ REFERENCES

(1) Mauderly, J. L.; Chow, J. C. Health effects of organic aerosols. *Inhalation Toxicol.* **2008**, *20*, 257−288.

(2) Atkinson, R. W.; Mills, I. C.; Walton, H. A.; Anderson, H. R. Fine particle components and health—a systematic review and meta-analysis of epidemiological time series studies of daily mortality and hospital admissions. *J. Exposure Sci. Environ. Epidemiol.* **2015**, *25*, 208−214.

(3) Jimenez, J. L.; Canagaratna, M. R.; Donahue, N. M.; Prevot, A. S. H.; Zhang, Q.; Kroll, J. H.; DeCarlo, P. F.; Allan, J. D.; Coe, H.; Ng, N. L.; et al. Evolution of Organic Aerosols in the Atmosphere. *Science* **2009**, *326*, 1525−1529.

(4) Hallquist, M.; Wenger, J. C.; Baltensperger, U.; Rudich, Y.; Simpson, D.; Claeys, M.; Dommen, J.; Donahue, N. M.; George, C.; Goldstein, A. H.; et al. The Formation, Properties and Impact of Secondary Organic Aerosol: Current and Emerging Issues. *Atmos. Chem. Phys.* **2009**, *9*, 5155−5236.

(5) Fard, M. M.; Krieger, U. K.; Peter, T. Shortwave radiative impact of liquid−liquid phase separation in brown carbon aerosols. *Atmos. Chem. Phys.* **2018**, *18*, 13511−13530.

(6) Slade, J. H.; Shiraiwa, M.; Arangio, A.; Su, H.; Pöschl, U.; Wang, J.; Knopf, D. A. Cloud droplet activation through oxidation of organic aerosol influenced by temperature and particle phase state. *Geophys. Res. Lett.* **2017**, *44*, 1583−1591.

(7) Schmedding, R.; Rasool, Q. Z.; Zhang, Y.; Pye, H. O. T.; Zhang, H.; Chen, Y.; Surratt, J. D.; Lopez-Hilfiker, F. D.; Thornton, J. A.; Goldstein, A. H.; et al. Predicting secondary organic aerosol phase state and viscosity and its effect on multiphase chemistry in a regional-scale air quality model. *Atmos. Chem. Phys.* **2020**, *20*, 8201−8225.

(8) Marcolli, C.; Krieger, U. K. Phase Changes during Hygroscopic Cycles of Mixed Organic/Inorganic Model Systems of Tropospheric Aerosols. *J. Phys. Chem. A* **2006**, *110*, 1881−1893.

(9) Zuend, A.; Marcolli, C.; Peter, T.; Seinfeld, J. H. Computation of liquid-liquid equilibria and phase stabilities: implications for RH-dependent gas/particle partitioning of organic-inorganic aerosols. *Atmos. Chem. Phys.* **2010**, *10*, 7795−7820.

(10) You, Y.; Renbaum-Wolff, L.; Bertram, A. K. Liquid−liquid phase separation in particles containing organics mixed with ammonium sulfate, ammonium bisulfate, ammonium nitrate or sodium chloride. *Atmos. Chem. Phys.* **2013**, *13*, 11723−11734.

(11) You, Y.; Smith, M. L.; Song, M. J.; Martin, S. T.; Bertram, A. K. Liquid-liquid phase separation in atmospherically relevant particles consisting of organic species and inorganic salts. *Int. Rev. Phys. Chem.* **2014**, *33*, 43−77.

(12) Losey, D. J.; Ott, E.-J. E.; Freedman, M. A. Effects of High Acidity on Phase Transitions of an Organic Aerosol. *J. Phys. Chem. A* **2018**, *122*, 3819−3828.

(13) Freedman, M. A.; Ott, E. J. E.; Marak, K. E. Role of pH in Aerosol Processes and Measurement Challenges. *J. Phys. Chem. A* **2019**, *123*, 1275−1284.

(14) Freedman, M. A. Liquid−Liquid Phase Separation in Supermicrometer and Submicrometer Aerosol Particles. *Acc. Chem. Res.* **2020**, *53*, 1102−1110.

(15) Parsons, M. T.; Riffell, J. L.; Bertram, A. K. Crystallization of aqueous inorganic-malonic acid particles: Nucleation rates, dependence on size, and dependence on the ammonium-to-sulfate. *J. Phys. Chem. A* **2006**, *110*, 8108−8115.

(16) Ciobanu, V. G.; Marcolli, C.; Krieger, U. K.; Weers, U.; Peter, T. Liquid−Liquid Phase Separation in Mixed Organic/Inorganic Aerosol Particles. *J. Phys. Chem. A* **2009**, *113*, 10966−10978.

(17) Bertram, A. K.; Martin, S. T.; Hanna, S. J.; Smith, M. L.; Bodsworth, A.; Chen, Q.; Kuwata, M.; Liu, A.; You, Y.; Zorn, S. R. Predicting the relative humidities of liquid-liquid phase separation, efflorescence, and deliquescence of mixed particles of ammonium sulfate, organic material, and water using the organic-to-sulfate mass ratio of the particle and the oxygen-to-carbon elemental ratio of the organic component. *Atmos. Chem. Phys.* **2011**, *11*, 10995−11006.

(18) You, Y.; Renbaum-Wolff, L.; Carreras-Sospedra, M.; Hanna, S. J.; Hiranuma, N.; Kamal, S.; Smith, M. L.; Zhang, X.; Weber, R. J.; Shilling, J. E.; et al. Images reveal that atmospheric particles can undergo liquid−liquid phase separations. *Proc. Natl. Acad. Sci. U.S.A.* **2012**, *109*, 13188−13193.

(19) Rafferty, A.; Gorkowski, K.; Zuend, A.; Preston, T. C. Optical deformation of single aerosol particles. *Proc. Natl. Acad. Sci. U.S.A.* **2019**, *116*, 19880−19886.

(20) Ohno, P. E.; Qin, Y.; Ye, J.; Wang, J.; Bertram, A. K.; Martin, S. T. Fluorescence Aerosol Flow Tube Spectroscopy to Detect Liquid−Liquid Phase Separation. *ACS Earth Space Chem.* **2021**, *5*, 1223−1232.

(21) Chen, Q.; Heald, C. L.; Jimenez, J. L.; Canagaratna, M. R.; Zhang, Q.; He, L.-Y.; Huang, X.-F.; Campuzano-Jost, P.; Palm, B. B.; Poulain, L.; et al. Elemental composition of organic aerosol: The gap between ambient and laboratory measurements. *Geophys. Res. Lett.* **2015**, *42*, 4182−4189.

(22) Chang, Y. S.; Abimannan, S.; Chiao, H. T.; Lin, C. Y.; Huang, Y. P. An ensemble learning based hybrid model and framework for air pollution forecasting. *Environ. Sci. Pollut. Res.* **2020**, *27*, 38155−38168.

(23) Xayasouk, T.; Lee, H.; Lee, G. Air Pollution Prediction Using Long Short-Term Memory (LSTM) and Deep Autoencoder (DAE) Models. *Sustainability* **2020**, *12*, No. 2570.

(24) Pak, U.; Ma, J.; Ryu, U.; Ryom, K.; Juhyok, U.; Pak, K.; Pak, C. Deep learning-based PM2.5 prediction considering the spatiotemporal correlations: A case study of Beijing, China. *Sci. Total Environ.* **2020**, *699*, No. 133561.

(25) Pak, U.; Kim, C.; Ryu, U.; Sok, K.; Pak, S. A hybrid model based on convolutional neural networks and long short-term memory for ozone concentration prediction. *Air Qual., Atmos. Health* **2018**, *11*, 883−895.

(26) Freeman, B. S.; Taylor, G.; Gharabaghi, B.; The, J. Forecasting air quality time series using deep learning. *J. Air Waste Manage. Assoc.* **2018**, *68*, 866−886.

(27) Soh, P. W.; Chang, J. W.; Huang, J. W. Adaptive Deep Learning-Based Air Quality Prediction Model Using the Most Relevant Spatial-Temporal Relations. *IEEE Access* **2018**, *6*, 38186−38199.

(28) O'Brien, R. E.; Wang, B. B.; Kelly, S. T.; Lundt, N.; You, Y.; Bertram, A. K.; Leone, S. R.; Laskin, A.; Gilles, M. K. Liquid-Liquid Phase Separation in Aerosol Particles: Imaging at the Nanometer Scale. *Environ. Sci. Technol.* **2015**, *49*, 4995−5002.

(29) McDonald, B. C.; de Gouw, J. A.; Gilman, J. B.; Jathar, S. H.; Akherati, A.; Cappa, C. D.; Jimenez, J. L.; Lee-Taylor, J.; Hayes, P. L.;

McKeen, S. A.; et al. Volatile chemical products emerging as largest petrochemical source of urban organic emissions. *Science* **2018**, *359*, 760−764.
(30) Colberg, C. A.; Luo, B. P.; Wernli, H.; Koop, T.; Peter, T. A novel model to predict the physical state of atmospheric H_2SO_4/NH_3/H_2O aerosol particles. *Atmos. Chem. Phys.* **2003**, *3*, 909−924.
(31) Gao, Y.; Chen, S. B.; Yu, L. E. Efflorescence Relative Humidity for Ammonium Sulfate Particles. *J. Phys. Chem. A* **2006**, *110*, 7602−7608.
(32) Wu, L.; Li, X.; Ro, C.-U. Hygroscopic behavior of ammonium sulfate, ammonium nitrate, and their mixture particles. *Asian J. Atmos. Environ.* **2019**, *13*, 196−211.
(33) Sun, J.; Liu, L.; Xu, L.; Wang, Y.; Wu, Z.; Hu, M.; Shi, Z.; Li, Y.; Zhang, X.; Chen, J.; et al. Key role of nitrate in phase transitions of urban particles: implications of important reactive surfaces for secondary aerosol formation. *J. Geophys. Res.: Atmos.* **2018**, *123*, 1234−1243.
(34) Beardsley, R. L.; Jang, M. Simulating the SOA Formation of Isoprene from Partitioning and Aerosol Phase Reactions in the Presence of Inorganics. *Atmos. Chem. Phys.* **2016**, *16*, 5993−6009.
(35) Jiang, H.; Jang, M.; Yu, Z. Dithiothreitol activity by particulate oxidizers of SOA produced from photooxidation of hydrocarbons under varied NO_x levels. *Atmos. Chem. Phys.* **2017**, *17*, 9965−9977.
(36) Yu, Z. C.; Jang, M.; Sabo-Attwood, T.; Robinson, S. E.; Jiang, H. H. Prediction of Delivery of Organic Aerosols onto Air-liquid Interface Cells in Vitro Using an Electrostatic Precipitator. *Toxicol. In Vitro* **2017**, *42*, 319−328.
(37) Yu, Z.; Jang, M. Atmospheric Processes of Aromatic Hydrocarbons in the Presence of Mineral Dust Particles in an Urban Environment. *ACS Earth Space Chem.* **2019**, *3*, 2404−2414.
(38) Zhou, C. F.; Jang, M.; Yu, Z. C. Simulation of SOA Formation From the Photooxidation of Monoalkylbenzenes in the Presence of Aqueous Aerosols Containing Electrolytes Under Various NO_x Levels. *Atmos. Chem. Phys.* **2019**, *19*, 5719−5735.
(39) Canagaratna, M. R.; Jimenez, J. L.; Kroll, J. H.; Chen, Q.; Kessler, S. H.; Massoli, P.; Hildebrandt Ruiz, L.; Fortner, E.; Williams, L. R.; Wilson, K. R.; et al. Elemental Ratio Measurements of Organic Compounds using Aerosol Mass Spectrometry: Characterization, Improved Calibration, and Implications. *Atmos. Chem. Phys.* **2015**, *15*, 253−272.
(40) Zhao, D. F.; Schmitt, S. H.; Wang, M. J.; Acir, I. H.; Tillmann, R.; Tan, Z. F.; Novelli, A.; Fuchs, H.; Pullinen, I.; Wegener, R.; et al. Effects of NO_x and SO_2 on the secondary organic aerosol formation from photooxidation of alpha-pinene and limonene. *Atmos. Chem. Phys.* **2018**, *18*, 1611−1628.
(41) Gao, Y.; Yu, L. E.; Chen, S. B. Efflorescence relative humidity of mixed sodium chloride and sodium sulfate particles. *J. Phys. Chem. A* **2007**, *111*, 10660−10666.
(42) Schlenker, J. C.; Malinowski, A.; Martin, S. T.; Hung, H.-M.; Rudich, Y. Crystals formed at 293 K by aqueous sulfate− nitrate− ammonium− proton aerosol particles. *J. Phys. Chem. A* **2004**, *108*, 9375−9383.
(43) Higgins, J. S.; Lipson, J. E.; White, R. P. A simple approach to polymer mixture miscibility. *Philos. Trans. R. Soc., A* **2010**, *368*, 1009−1025.
(44) Khan, I.; Poh, B. Effect of molecular weight and testing rate on adhesion property of pressure-sensitive adhesives prepared from epoxidized natural rubber. *Mater. Des.* **2011**, *32*, 2513−2519.
(45) Song, M.; Marcolli, C.; Krieger, U.; Zuend, A.; Peter, T. Liquid-liquid phase separation in aerosol particles: Dependence on O: C, organic functionalities, and compositional complexity. *Geophys. Res. Lett.* **2012**, *39*, No. L19801.
(46) Song, M.; Marcolli, C.; Krieger, U. K.; Zuend, A.; Peter, T. Liquid-liquid phase separation and morphology of internally mixed dicarboxylic acids/ammonium sulfate/water particles. *Atmos. Chem. Phys.* **2012**, *12*, 2691−2712.
(47) You, Y.; Bertram, A. K. Effects of molecular weight and temperature on liquid−liquid phase separation in particles containing organic species and inorganic salts. *Atmos. Chem. Phys.* **2015**, *15*, 1351−1365.
(48) Han, S.; Jang, M. Simulating the impact of gas-wall partitioning on SOA formation using the explicit gas mechanism integrated with aqueous reactions containing electrolytes. *Sci. Total Environ.* **2020**, *748*, No. 141360.
(49) Yu, Z.; Jang, M.; Zhang, T.; Madhu, A.; Han, S. Simulation of Monoterpene SOA Formation by Multiphase Reactions Using Explicit Mechanisms. *ACS Earth Space Chem.* **2021**, *5*, 1455−1467.
(50) Ripoll, A.; Minguillon, M. C.; Pey, J.; Jimenez, J. L.; Day, D. A.; Sosedova, Y.; Canonaco, F.; Prevot, A. S. H.; Querol, X.; Alastuey, A. Long-term real-time chemical characterization of submicron aerosols at Montsec (southern Pyrenees, 1570 m a.s.l.). *Atmos. Chem. Phys.* **2015**, *15*, 2935−2951.
(51) Dao, X.; Lin, Y.-C.; Cao, F.; Di, S.-Y.; Hong, Y.; Xing, G.; Li, J.; Fu, P.; Zhang, Y.-L. Introduction to the national aerosol chemical composition monitoring network of China: objectives, current status, and outlook. *Bull. Am. Meteorol. Soc.* **2019**, *100*, ES337−ES351.
(52) Sun, Y.; Wang, Z.; Dong, H.; Yang, T.; Li, J.; Pan, X.; Chen, P.; Jayne, J. T. Characterization of summer organic and inorganic aerosols in Beijing, China with an Aerosol Chemical Speciation Monitor. *Atmos. Environ.* **2012**, *51*, 250−259.
(53) Carlton, A. G.; Wiedinmyer, C.; Kroll, J. H. A review of Secondary Organic Aerosol (SOA) formation from isoprene. *Atmos. Chem. Phys.* **2009**, *9*, 4987−5005.
(54) McNeill, V. F. Aqueous Organic Chemistry in the Atmosphere: Sources and Chemical Processing of Organic Aerosols. *Environ. Sci. Technol.* **2015**, *49*, 1237−1244.
(55) Bateman, A. P.; Bertram, A. K.; Martin, S. T. Hygroscopic Influence on the Semisolid-to-Liquid Transition of Secondary Organic Materials. *J. Phys. Chem. A* **2015**, *119*, 4386−4395.
(56) Nguyen, T. B.; Roach, P. J.; Laskin, J.; Laskin, A.; Nizkorodov, S. A. Effect of humidity on the composition of isoprene photooxidation secondary organic aerosol. *Atmos. Chem. Phys.* **2011**, *11*, 6931−6944.
(57) Kourtchev, I.; Hellebust, S.; Bell, J. M.; O'Connor, I. P.; Healy, R. M.; Allanic, A.; Healy, D.; Wenger, J. C.; Sodeau, J. R. The use of polar organic compounds to estimate the contribution of domestic solid fuel combustion and biogenic sources to ambient levels of organic carbon and PM2.5 in Cork Harbour, Ireland. *Sci. Total Environ.* **2011**, *409*, 2143−2155.
(58) Ervens, B.; Turpin, B. J.; Weber, R. J. Secondary organic aerosol formation in cloud droplets and aqueous particles (aqSOA): a review of laboratory, field and model studies. *Atmos. Chem. Phys.* **2011**, *11*, 11069−11102.
(59) Pye, H. O. T.; Nenes, A.; Alexander, B.; Ault, A. P.; Barth, M. C.; Clegg, S. L.; Collett, J. L., Jr.; Fahey, K. M.; Hennigan, C. J.; Herrmann, H.; et al. The acidity of atmospheric particles and clouds. *Atmos. Chem. Phys.* **2020**, *20*, 4809−4888.
(60) Altaf, M. B.; Zuend, A.; Freedman, M. A. Role of nucleation mechanism on the size dependent morphology of organic aerosol. *Chem. Commun.* **2016**, *52*, 9220−9223.

https://doi.org/10.1021/acs.jpca.1c06773
J. Phys. Chem. A 2021, 125, 10198−10206